Hindawi
International Journal of Geophysics
Volume 2023, Article ID 1891759, 18 pages
https://doi.org/10.1155/2023/1891759

*Research Article*

# Hydrological Evaluation of the Groundwater Potential in the Fractured Karoo Aquifer Using Magnetic and Electrical Resistivity Methods: Case Study of the Balfour Formation, Alice, South Africa

**Gbenga Olamide Adesola, Oswald Gwavava, and Kuiwu Liu**

*Department of Geology, University of Fort Hare, Private Bag X1314, Alice 5700, South Africa*

Correspondence should be addressed to Gbenga Olamide Adesola; gbengaadesola@gmail.com

Received 24 April 2023; Revised 21 July 2023; Accepted 23 August 2023; Published 6 September 2023

Academic Editor: Sándor Szalai



The study is aimed at evaluating the groundwater accumulations present in Alice using magnetic and electrical resistivity measurements to examine the trends of structural elements and characterize the groundwater resource for borehole drilling. The magnetic maps show a low magnetic linear structure moving northwest to southeast direction, which may be caused by fractures. The linear high intensities were probably caused by dolerite dykes, while dolerite sills caused broader high-intensity areas. The depth slices show that the near-surface magnetic structures are visible to a depth of about 19 m, and the deep-seated structures are found at a depth of about 31 m, possibly deeper. Twenty-five vertical electrical soundings (VES) of the Schlumberger array were measured with AB/2 varying between 1.5 m and 250 m across the study area. The VES interpretation showed four geoelectric layers composed of HK and HA curve types. The geoelectric layer's thicknesses are (1) topsoil from 0.4 to 1.8 m, (2) weathered layer from 0.8 to 17.5 m, and (3) weathered/fractured layer from 9.9 to 143.9 m; the third layer could be the productive water-bearing zones, and (4) bedrock layer has an infinite thickness. The layers have resistivity values of 20-5752 Ωm, 3-51 Ωm, 136-352 Ωm, and 44-60428 Ωm, respectively. A correlation of the VES with the borehole log indicated a well-matched result. The magnetic and electrical resistivity surveys provided a detailed subsurface structure and helped identify possible fractures that could act as a passage for groundwater.

## 1. Introduction

Groundwater resource is becoming essential and accounts for a significant proportion of the water used for various purposes [1]. Many rural communities rely on dams and rivers' surface water supplies, which might be completely or almost dry during dry seasons [2]. Groundwater is mostly odorless and contains low dissolved solids [3]. The benefits of groundwater, being the source of potable water, cannot be underestimated, mainly in places whereby the population is predominantly rural, and demand is distributed across wide areas [4]. Finding sustainable, hygienic, and potable water is a big challenge that never ends because it promotes the development of every community [5]. Surface water is becoming increasingly scarce due to the strain of industrial growth in several areas of the globe. Due to this, water scarcity is now the third most significant global problem since freshwater makes up only 3% of all water on Earth [6]. Groundwater is the primary source of drinking water for over 60% of people worldwide [7]. It makes up roughly 40% of the total water supply by the government in the UK, additionally about 99% in Denmark, 60% in the USA [7, 8], and approximately 80% in Germany [7]. In South Africa, 22% of communities rely solely on groundwater; another 34% combine it with surface water [9].

The limited and uneven water distribution in South Africa is severely impacted by climate change and the development of invasive alien plant species [10]. Owing to population growth and migration, the development of rural areas

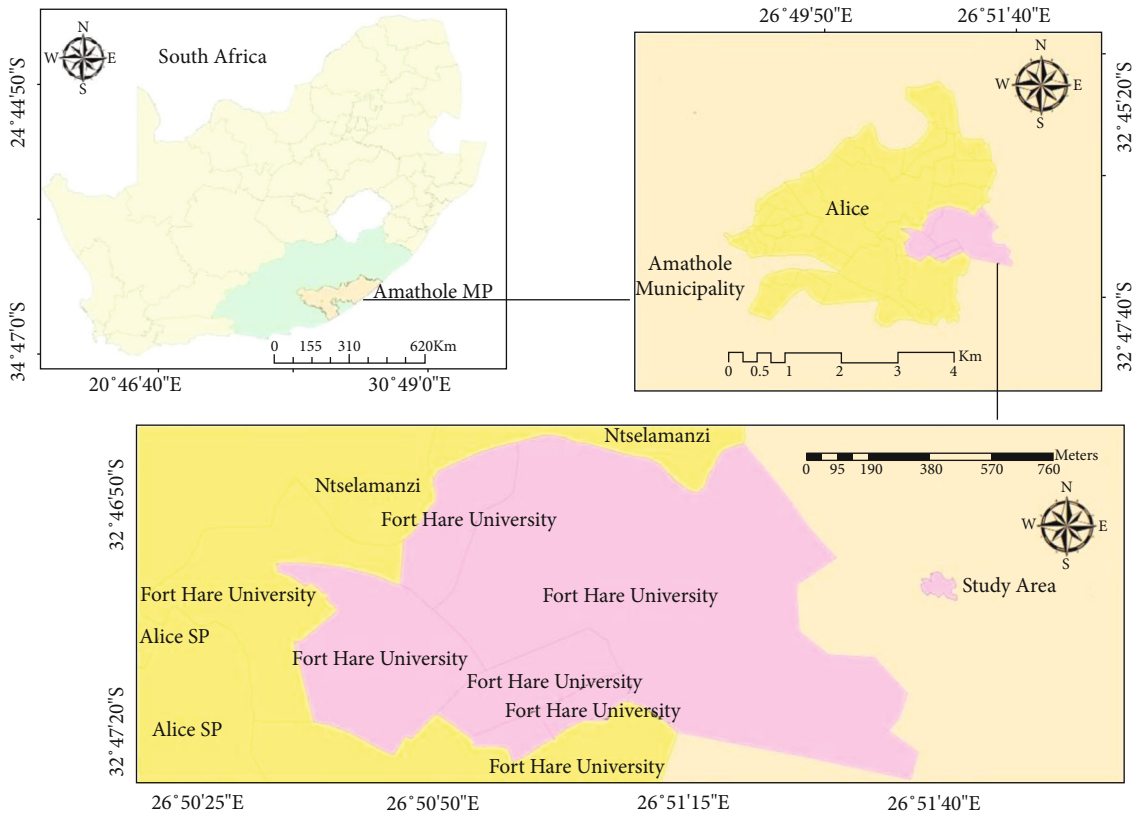


Figure 1: Simplified map of the study area.

puts a strain on South Africa's water system. According to [11], nine million South Africans are not provided with drinkable water, and one-third of the country's population lacks access to water infrastructure. In addition, about five provinces in South Africa were announced as disaster zones in 2015 as a result of the severe drought that unfortunately hit the nation. Several countries in semiarid and arid areas, including South Africa, are classified as water-stressed [11] and rely on groundwater as their primary water source for numerous purposes. Studying the properties of aquifers and the pattern of groundwater movement is vital for the country's water resource development.

Groundwater investigation is often based on assessing the hydrological indicators and validation using a geological and geophysical application in hydrology [12]. Fault zones, lineaments, and fractures change the characteristics of a hydrogeological medium [13]. Several studies have established that drilling wells through faults or cracks increase borehole yield [14–16]. [17] notes that the magnetic technique is the fast and most affordable method for mapping the weathered/fractured basement and investigating surface-to-subsurface geological formations. Numerous authors have successfully applied the magnetic technique to map the subsurface features [17–19]. Electromagnetic, electrical resistivity, or seismic surveys are usually conducted after a magnetic survey to obtain accurate subsurface information. The electrical resistivity technique is the most often utilized geophysical method for groundwater studies, among others, as it could give a strong response under the existing subsurface conditions [20, 21].

The integrated applications of magnetic and electrical resistivity techniques provide a better understanding of subsurface geology [22]. Many researchers have used magnetic and resistivity methods as a combined geophysical tool to efficiently investigate groundwater [23–25]. Ground magnetic survey and vertical electrical sounding (VES) were combined to understand the subsurface geology and ascertain groundwater availability in Alice. Furthermore, this was done to show the benefits of magnetic and resistivity methods as proficient geophysical tools for investigating deep and shallow aquifers.

One of the provinces struggling to provide clean water to its residents is the Eastern Cape, where Alice is situated (Figure 1). There is essentially no groundwater in most aquifers [26]. The municipality supplies Alice with piped water every day. There was no water supply scarcity from the reservoir in the municipality until the reservoir turned out to be the major source of water supply to recently developed neighborhoods near Alice. Previous studies conducted in Alice focused on the contaminant delineation of a landfill site [27] using combined induced polarization and electrical resistivity methods and the characterization of the weathered/fractured aquifer using geological mapping, data collection, and borehole drilling and logging [28]. To date, no studies have been conducted to evaluate Alice's groundwater resources. This knowledge gap could hinder efficient groundwater production. To better understand Alice's groundwater resources, a thorough investigation is required to know the overburden thickness and depth to bedrock and vertical and horizontal changes in electrical resistivity with depth and select subsurface aquifer zones for borehole drilling.

## 2. Geology

The Karoo Basin is a sedimentary basin that covers about 600,000 km$^2$ of central and southern South Africa. Its sedimentation occurred about 300 million years ago during the late Carboniferous, up until the breakup of Gondwana in the Middle Jurassic. The breakup was mainly because of the deposition of a large igneous province [29], whereby dolerite sills and dykes intruded the surrounding sediments and induced the formation of fractures. The dolerite sills and dykes are now responsible for the recharge and drainage patterns, as well as controlling the morphology and influencing the emergence of many seepages and springs [28]. [30] reported that this basin is a retro-arc foreland basin, which occurred when the Paleo-pacific plate underwent subduction at a shallow angle underneath Gondwana. The Karoo Supergroup is stratigraphically divided into Dwyka, Ecca, Beaufort, Stormberg, and Drakensberg Groups [31]. The groups are mainly composed of sedimentary sequences, apart from the Drakensberg Group, comprising volcanic rocks [31]. [32] reported that the Karoo Basin protects a stratum of glaciomarine to terrestrial sequences that are formed in a diversity of tectonically influenced depositories under increasingly arid climatic settings. The southern part of the depositional environment of the Karoo varied from glacial (Dwyka) to fluvial (Ecca) over time.

The Dwyka Group is formed at the bottom of the Karoo Basin (Table 1). In the southern part of the Karoo, the group unconformably overlies the Cape Supergroup [33]. The group is 600 m-750 m thick, comprising diamictites and shales [34]. It is roughly 2340 m thick [34]. It comprises six formations, which are Prince Albert, Whitehill, Collingham, Ripon, Fort Brown, and Waterford Formations [28]. The Beaufort Group, consisting of the lower Adelaide Subgroup and the upper Tarkastad Subgroup [28], comprises alternating sandstones and mudrocks and has attained a thickness above 500 m and a surface area of about 200,000 km$^2$ [34]. The group's age ranges from the Middle Permian to the Middle Triassic period [35].

The study area is situated in the Balfour Formation within the Beaufort Group. It is made up of a succession of sedimentary rocks, including a succession of mudstones with subordinate interbedded sandstones, siltstone, and shale. These rocks were eventually intruded by the dolerites in the Karoo, forming sills and dykes [36]. The variation in its lithology is characterized by alternating sandstone-rich and mudstone-rich members [37]. This formation is divided into five stratigraphic members, namely, Oudeberg, Daggaboersnek, Barberskrans, Elandsberg, and Palingkloof [35]. Alice is geologically located in the Daggaboersnek Member (Figure 2). The Daggaboersnek Member is made up of sandstones with mudrock intercalations. According to [38], shale, siltstone, sandstone, and mudstones make up the majority of the low-permeability Karoo aquifers. Many boreholes drilled in the Karoo Formation are recorded to be of low yields [26].

## 3. Materials and Methods

*3.1. Magnetic Study.* Magnetic data were acquired from 8458 points in Alice using the G-857 magnetometer. Two magnetometers were used for the ground magnetic survey. The magnetometers were checked to know whether they both measured similar values at a given time in the same place. One magnetometer was fixed at the base station to account for diurnal variation. There were no magnetic objects in the area where this base station was located. The base station readings were taken at an interval of 30 s. The magnetic intensity of the research area was measured using a second magnetometer along the traverse. The intertraverse spacing was 20 m. Readings along the traverses were recorded at an interval of 5 s. These traverses were located far from significant metallic objects. The magnetic readings and time of the recording were taken and stored automatically by the magnetometer. The time of recording is needed for the correction of diurnal variations. The Garmin GPS was mounted on the G-857 magnetometer nonmetallic sensor pole, and it was configured to record locations when taking magnetic readings along the traverse.

*3.1.1. Magnetic Data Analysis.* The ground magnetic data were processed using Geosoft software, Oasis Montaj 9.10, for filtering and enhancement to improve the interpretive power of the magnetic data. Data enhancements (i.e., reduced magnetic pole, total horizontal derivative, vertical derivative, and analytical signal) were applied to the residual magnetic data to identify the edges of geological features and enhance deeper magnetic sources [41, 42]. Magnetic depth slicing was successfully conducted with the aid of GETECH GETGRID software. The magnetic results are displayed using spatial maps ("Reduced to the pole," "Total horizontal derivative," "Vertical derivative," and "Analytical signal" sections). The enhancement techniques are summarized below.

*(1) Reduced to the Pole (RTP).* The analysis of the residual magnetic field intensity map is generally inaccurate due to the movement of magnetic anomalies away from their magnetic sources [41]. The magnetic inclination of 63.63° and declination of -28.02° were applied to the total magnetic field map after removing the diurnal variation to produce the RTP map [43]. The RTP map allows the elimination of anomalous skewness while maintaining the data configuration [44]. This computation process aligns the boundaries of the magnetic anomalies with their buried sources [45]. This was accomplished by using Equation (1) to determine the differentiation of the source components in the vertical direction [45].

$$\Delta T_y(r) = \frac{\delta^2}{\delta y^2} \iint_{-\infty}^{\infty} \Delta T(r) \cdot \delta\rho \cdot \delta b, \tag{1}$$

where $T_y(r)$ = RTP magnetic anomaly depends on the vertical magnetization ($y$), $r$ is the radius of the magnetization field from the magnetic source to the point of observation, $\rho$ is the direction of the anomalous magnetization, and $b$ is the direction of the magnetic field of the earth magnetic field.

*(2) Analytical Signal (AS) Mapping.* The analytical signal (AS) is produced by combining the vertical and horizontal gradients of magnetic anomalies. The analytical signal has both direction and amplitude. However, the analytical signal is generally defined by its "amplitude function" (i.e., the

Table 1: Lithostratigraphic subdivisions of the Karoo Supergroup [40].

| Supergroup | Group | Subgroup | Formation | Member | Lithology |
|---|---|---|---|---|---|
| Karoo | Stormberg | | Drakensberg | | Basalt<br>Pyroclastic deposits |
| | | | Clarens | | Sandstone |
| | | | Elliot | | Red mudstone<br>Sandstone |
| | | | Molteno | | Coarse sandstone<br>Khaki and grey shale<br>Coal measures |
| | Beaufort | Tarkastad | Burgersdorp | | Mudstone<br>Sandstone<br>Grey shale |
| | | | Katberg | | Sandstone<br>Red mudstone<br>Grey shale |
| | | Adelaide | Balfour | Palingkloof | Red mudstone<br>Sandstone<br>Grey shale |
| | | | | Elandsberg | Sandstone<br>Siltstone |
| | | | | Barberskrans | Sandstone<br>Khaki shale |
| | | | | Daggaboersnek | Grey shale<br>Sandstone<br>Siltstone |
| | | | | Oudeberg | Sandstone<br>Khaki shale |
| | Ecca | | Middleton | | Shale<br>Sandstone<br>Red mudstone |
| | | | Koonap | | Grey sandstone<br>Shale |
| | | | Waterford | | Sandstone<br>Shale |
| | | | Fort Brown | | Shale<br>Sandstone |
| | | | Ripon | | Sandstone<br>Shale |
| | | | Collingham | | Grey shale<br>Yellow claystone |
| | | | Whitehill | | Black shale<br>Chert |
| | | | Prince Albert | | Khaki shale |
| | | | Dwyka | | Diamictite<br>Tillite<br>Shale |

square root of the sum of the squares of the horizontal and vertical derivatives of the Earth's magnetic field) [46]. The data in the wavenumber domain was processed and filtered using an inverse fast Fourier transform (FFT) algorithm. The filter's capacity to provide a total value precisely over the magnetic source, as well as a depth estimate, makes it a suitable method for interpreting magnetic data [47]. [48] states that the benefit of this magnetic data enhancement technique is that it does not depend on specific preconceptions regarding the body's magnetization direction, and it usually has a positive amplitude function. The analytical signal was computed using the following equation:

$$A(x, y) = \sqrt{\left(\frac{\delta f}{\delta x}\right)^2 + \left(\frac{\delta f}{\delta y}\right)^2 + \left(\frac{\delta f}{\delta z}\right)^2}, \quad (2)$$

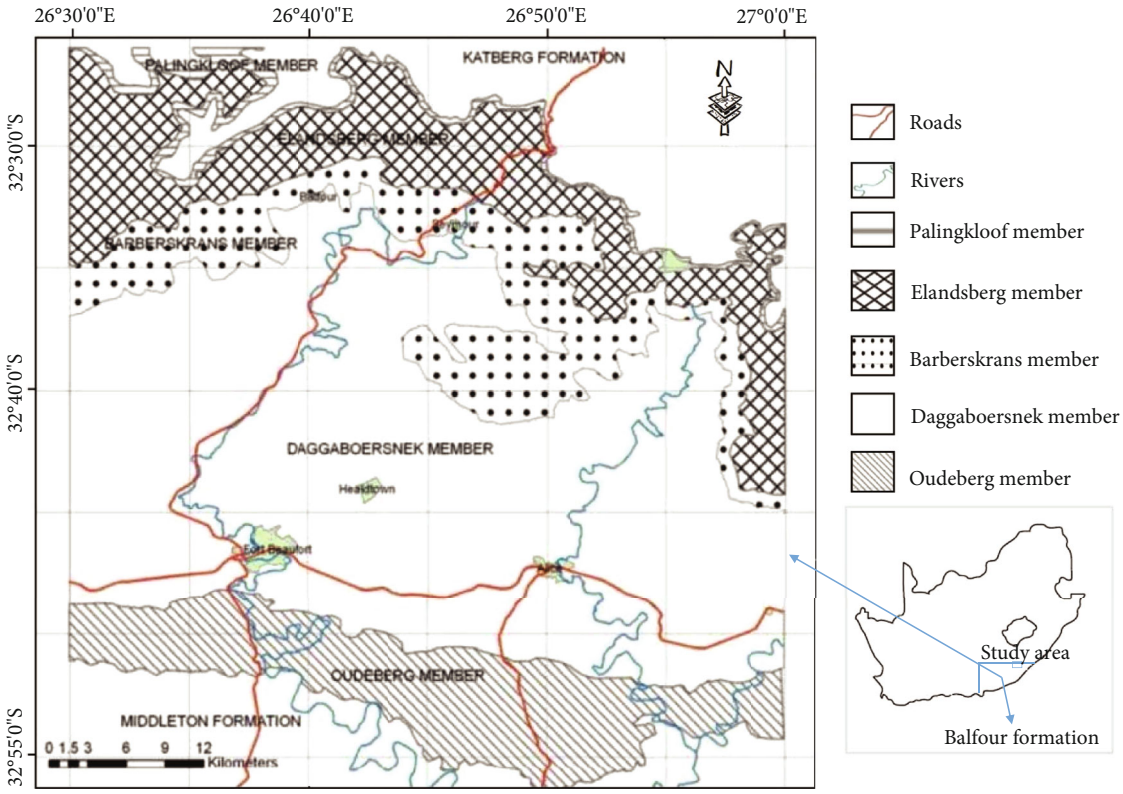


Figure 2: Detailed geological map of Alice [37, 39].

where $A(x, y)$ is the amplitude of the AS at $(x, y)$, $f$ is the observed magnetic field at $(x, y)$, and $x$, $y$, and $z$ are the edges of the magnetic structure.

*(3) First Vertical Derivative (FVD).* The vertical gradients of potential fields are potentially important in interpreting magnetic data because they map out linear structures such as dykes or faults [39]. [49] noted that the FVD technique is useful in enhancing magnetic anomalies caused by shallow sources, narrowing the size of the anomalies, and identifying the causative bodies precisely. The vertical derivative map responds very well to local effects than regional impacts, producing a sharper image than the total field magnetic map [49].

*(4) Total Horizontal Derivative (THD).* Horizontal derivatives (THD) are magnetic vector data that provide more information about the directional variations of the total magnetic field [50]. They are crucial in mapping linear features like dykes or fault zones from magnetic data [51]. Horizontal derivative maps are derivative products that point out discontinuities in anomalous patterns and textures. The Pythagorean sum of the gradients in orthogonal directions is used to compute an anomaly field's horizontal derivative. The horizontal gradient magnitude $\mathrm{THD}(x, y)$ for the magnetic field $F(x, y)$ is given by [52] as follows:

$$\mathrm{THD}(x, y) = \sqrt{\left(\frac{\delta f}{\delta x}\right)^2 + \left(\frac{\delta f}{\delta y}\right)^2}, \tag{3}$$

where $\mathrm{THD}(x, y)$ is the amplitude of the THD at $(x, y)$, $f$ is the observed magnetic field at $(x, y)$, and $x$ and $y$ are the edges of the magnetic structure.

*(5) Depth Slicing Technique.* This technique uses the linear filter to estimate the depth of the magnetic anomaly source as a plot of the gradient of the Earth's magnetic field all through the subsidence of the magnetic anomaly [50]. [39] noted that the magnetic signal is considered the outcome of several uncorrelated random processes, according to the Wiener filtering principle, which is the basis for depth slicing. Outlining the impacts of shallow magnetic sources from deeper magnetic sources enables the differentiation of many data components. The majority of magnetic anomalies seen at the surface typically come from shallow depths, whereas unclear magnetic anomalies generally come from deeper depths. The depth estimation is calculated using the following equation:

$$h = \frac{b}{-4\pi}, \tag{4}$$

where $h$ represents the depth of the anomalous body and $b$ represents the Nyquist wavenumber component's slope.

*3.2. Vertical Electrical Sounding Survey.* The fieldwork was done between April and May 2019. A geophysical investigation was conducted in Alice using ABEM Terrameter SAS 1000C resistivity equipment alongside four metal electrodes (a pair for electric potential and the other pair for electric


Figure 3: Vertical electrical sounding using Schlumberger configuration in Alice.

current flow measurements), cables, hammers, GPS, and measuring tapes (Figure 3). The vertical electrical sounding (VES) method using the Schlumberger electrode configuration (Figure 3), which is effective in the investigation of groundwater, was used for the resistivity measurements to determine the apparent resistivity [53]. The Schlumberger array is successfully utilized for groundwater studies because of its flexibility, easy interpretation, and durability of the instrument used for the survey [54]. The survey was completed at twenty-five (25) VES stations within the study area (Figure 4). Four electrodes were arranged collinearly, and two current electrodes, A and B, were used for deep current penetration (Figure 3) while measuring the potential difference using another pair of electrodes (M and N) [55]. The current electrodes (AB) were gradually moved outwardly, leaving the potential difference electrodes (MN) fixed to increase the depth range of the particular station being investigated. At some points, the ratio AB/MN became too large, which led to a drop in the potential difference values, making the readings inaccurate. Therefore, it was necessary to increase the potential difference electrodes (MN), and the distance between the electrodes was kept at MN ≤ AB/5 in order to provide accurate resistivity data. The potential difference readings from the instrument were maintained at a value greater than 5 mV. The current electrodes (AB/2) reached a distance of 250 m, while the potential electrodes (MN) started from 0.5 m and subsequently extended to a suitable distance as the current electrodes (AB) were moved symmetrically.

For the Schlumberger electrode configuration, the instrument measured the apparent resistivity ($\rho_a$) using the following equation:

$$\rho_a = k\left(\frac{\Delta v}{I}\right), \tag{5}$$

where $k$ is the geometric factor, $\Delta V$ is the potential difference, and $I$ is the electric current.

The geometric factor ($k$) for the Schlumberger array is calculated using the following equation:

$$k = \pi\left(\frac{S^2 - a^2/4}{a}\right), \tag{6}$$

where $s$ is the distance between two current electrodes AB and $a$ is the distance between two potential electrodes MN.

The results of the VES are presented as electrical sounding curves and geoelectric cross-sections.

*3.2.1. Data Analysis and Resistivity Interpretation.* The obtained VES data were analyzed with the aid of the partial curve matching technique and iteration modeling method using WINRESIST software to produce the geoelectric models and SURFER-10 software to generate the geoelectric sections [56]. The partial curve matching technique is based on a preliminary evaluation that provides the thickness and resistivity of different geoelectric layers [57]. The thickness, resistivity, and depth of a layer are taken into account when deciding if a layer is fractured or weathered, which makes the layer suitable for groundwater storage. The decision is accomplished by comparing each layer's resistivity measurements with the standard resistivity values of groundwater. The resistivity values of groundwater vary between 10 and 100 Ωm since the quantity of dissolved salts in groundwater lowers its resistivity [58]. The VES points with a layer having resistivity values between 10 and 200 Ωm, large thickness, and a depth greater than 30 m are therefore chosen, considering the water table and depths of the existing borehole from previous studies [26, 28].

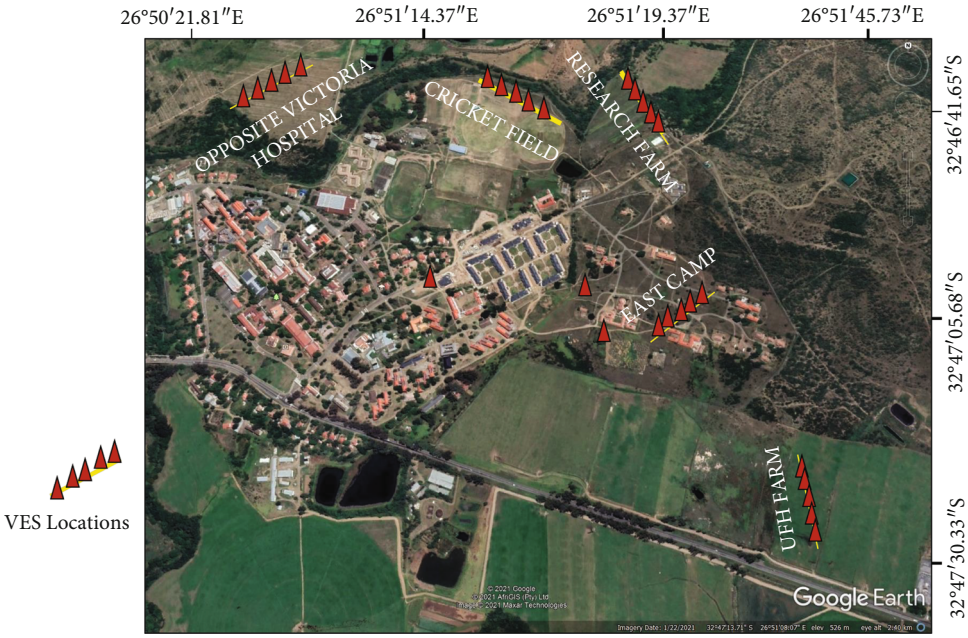


Figure 4: Satellite image of Alice displaying the VES locations (Google Earth).

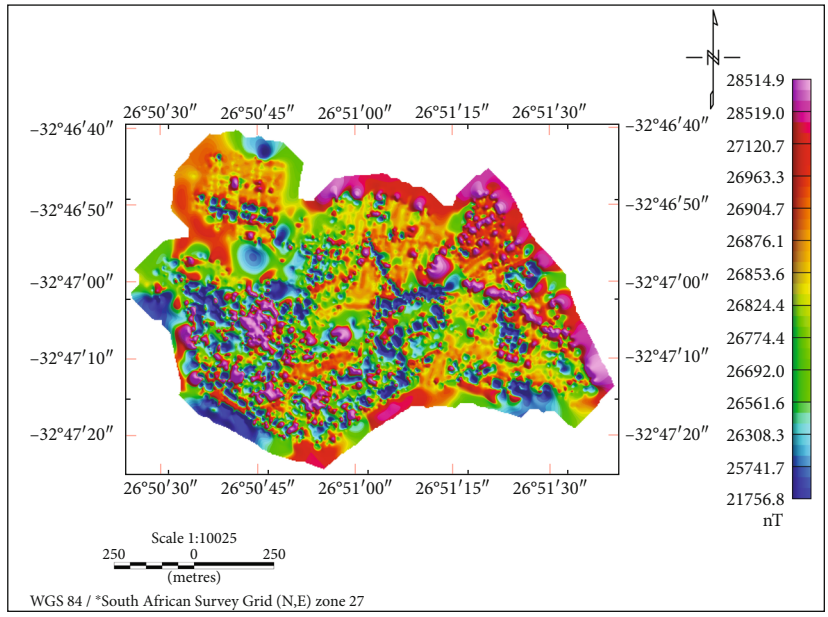


Figure 5: The residual magnetic map of the study area.

## 4. Results

The geophysical techniques of magnetic and electrical resistivity surveys were combined to examine the subsurface geological structures which influence the distribution of groundwater using magnetic data and evaluate the thickness of water-bearing areas and depth using the electrical resistivity data, hence identifying potential groundwater zones.

*4.1. Magnetic.* The results of the magnetic survey are presented in maps. The residual magnetic map is presented in Figure 5. The amplitude of the total magnetic map ranges from 21756.8 to 28514.9 nT. However, this map could not be accurately interpreted owing to the effect of the nonzero magnetic inclination. Therefore, it was reduced to the pole (RTP) and displayed as an RTP map in Figure 6.

*4.1.1. Reduced to the Pole (RTP).* The RTP map of Alice has a magnetic field intensity ranging between 21361.0 and 27735.7 nT (Figure 6). The sources of the remnant magnetization show the areas of tectonic stress observed in the northwestern, southwestern, central, and eastern parts of the study area. The RTP map displays a high magnetic intensity in the NE and SW parts, while a low magnetic intensity dominates the western parts. At the center of the RTP map, the magnetic

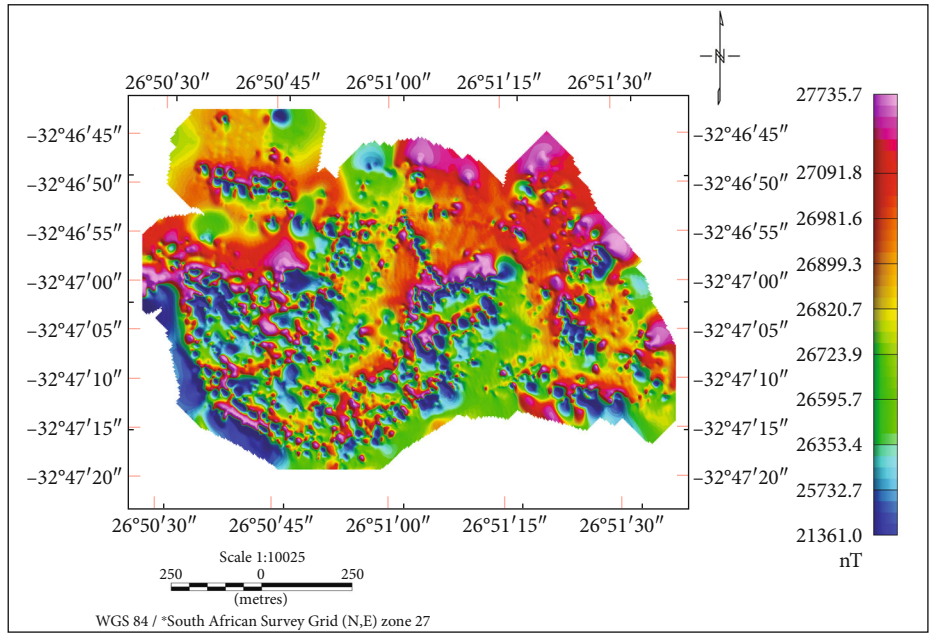


Figure 6: Reduced to the pole map of the study area.

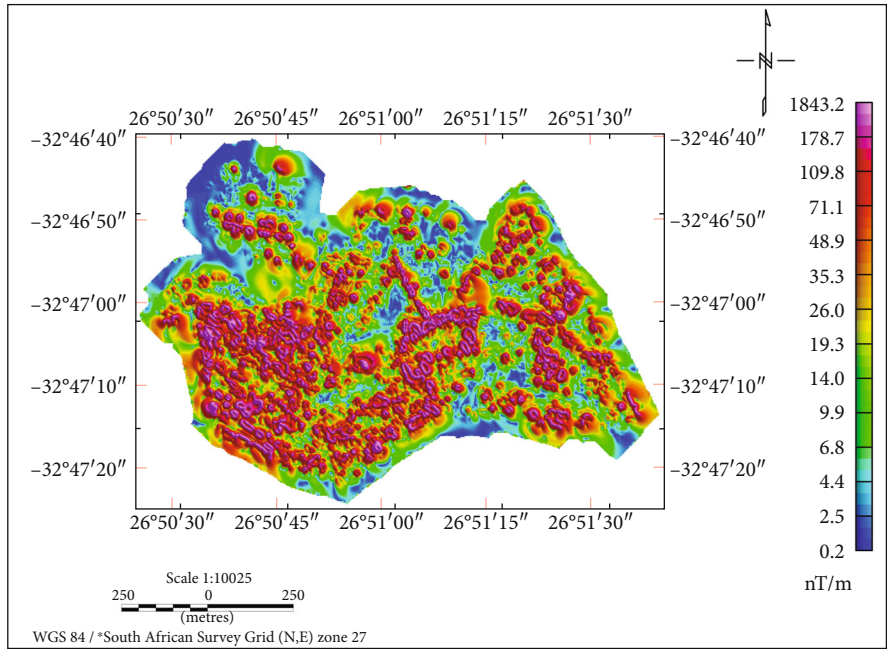


Figure 7: Total horizontal derivative (THD) map of the study area.

anomalies create a pair of narrow, low magnetic intensities that are nearly parallel to one another.

*4.1.2. Total Horizontal Derivative (THD).* A THD map (Figure 7) was produced to show the locations and orientations of the subsurface structures such as faults and fractures, which may control the flow path of groundwater. The THD map reveals the contact locations as peak amplitude anomalies with values varying from 0.2 to 1843.2 nT/m. The anomaly maxima, highlighted on the map as black lines, represent the identified contact locations. The high THD amplitude varying between 71.1 and 1843.2 nT/m correlates with the dolerite intrusions, specifically the parallel dykes trending west-east direction at the center and southwestern parts.

*4.1.3. First Vertical Derivative (FVD).* The FVD map (Figure 8) displays many magnetic features which indicate a ring-like shape. However, some linear structures indicate dolerite intrusions found in Karoo [59]. The peak amplitude anomalies on the map that represent the contact points have values varying between −1902 and 3628.3 nT/m.

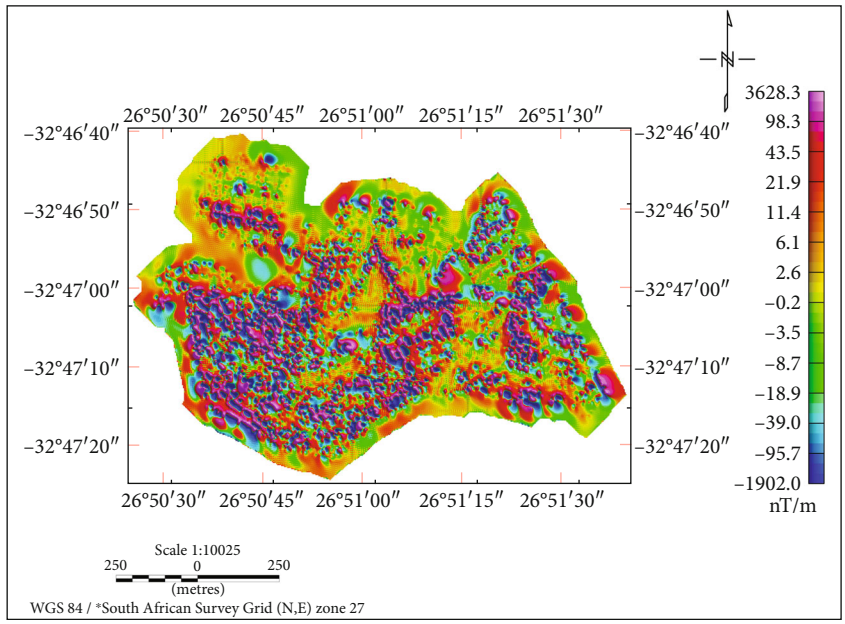


Figure 8: Vertical derivative magnetic map of the study area.

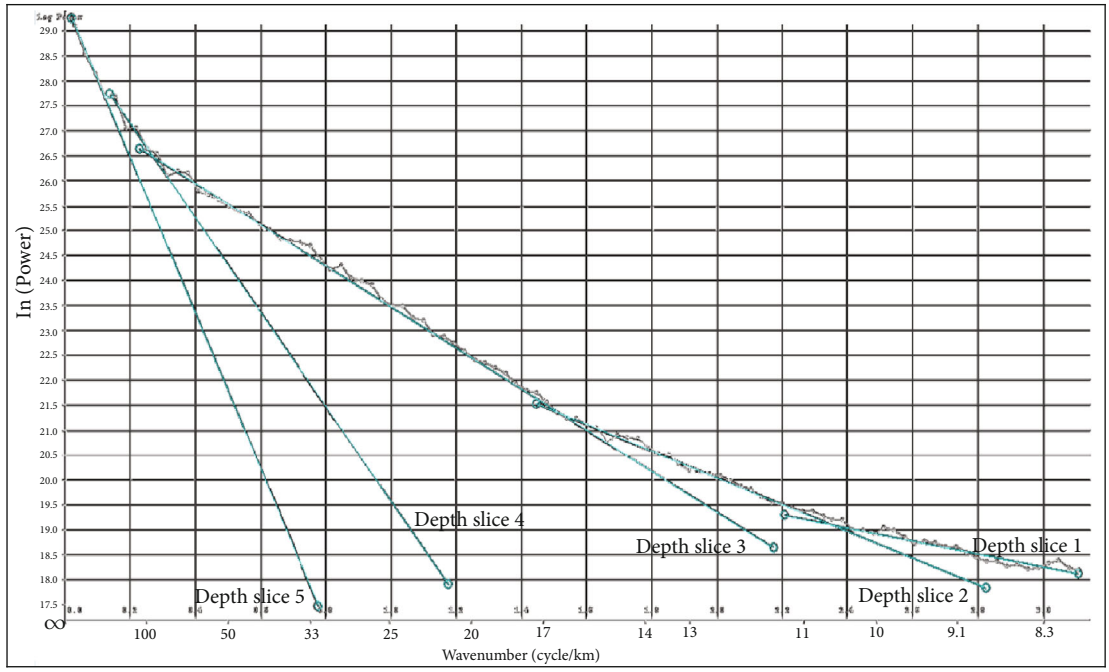


Figure 9: Magnetic power spectrum of the study area.

*4.1.4. Magnetic Spectrum Assessment and Depth Slicing.* The magnetic spectrum assessment was done to know the shape and depth of the magnetic source using the power spectrum result (Figure 9). The five main linear structures observed at depths 2.57 m, 5.31 m, 8.91 m, 18.1 m, and 30.8 m indicate magnetic anomalies due to shallow and deep-seated sources (Figure 10). Depth slice 1 reveals that the majority of the shallow magnetic anomalies are located at 2.57 m depth, whereas the anomalies are still visible in slice 2 up to 5.31 m depth. Slices 3 and 4 (8.19 m and 18.8 m, respectively) show broader sills, which are thought to feed the near-surface dykes. The slide 5 map (Figure 10(e)) does not show the narrow anomalies caused by shallow magnetic sources that can be seen on the depth slices 1 to 4 maps (Figures 10(a)–10(d)). This is due to the shallow sources' disappearance at a depth of about 31 m.

*4.2. Vertical Electrical Sounding (VES).* The VES interpretation showed four geoelectric layers, and the curves consist of HA and HK types. About 64% of the overall soundings are of the HA curve type, whereas 36% are of the HK type (Figure 11).

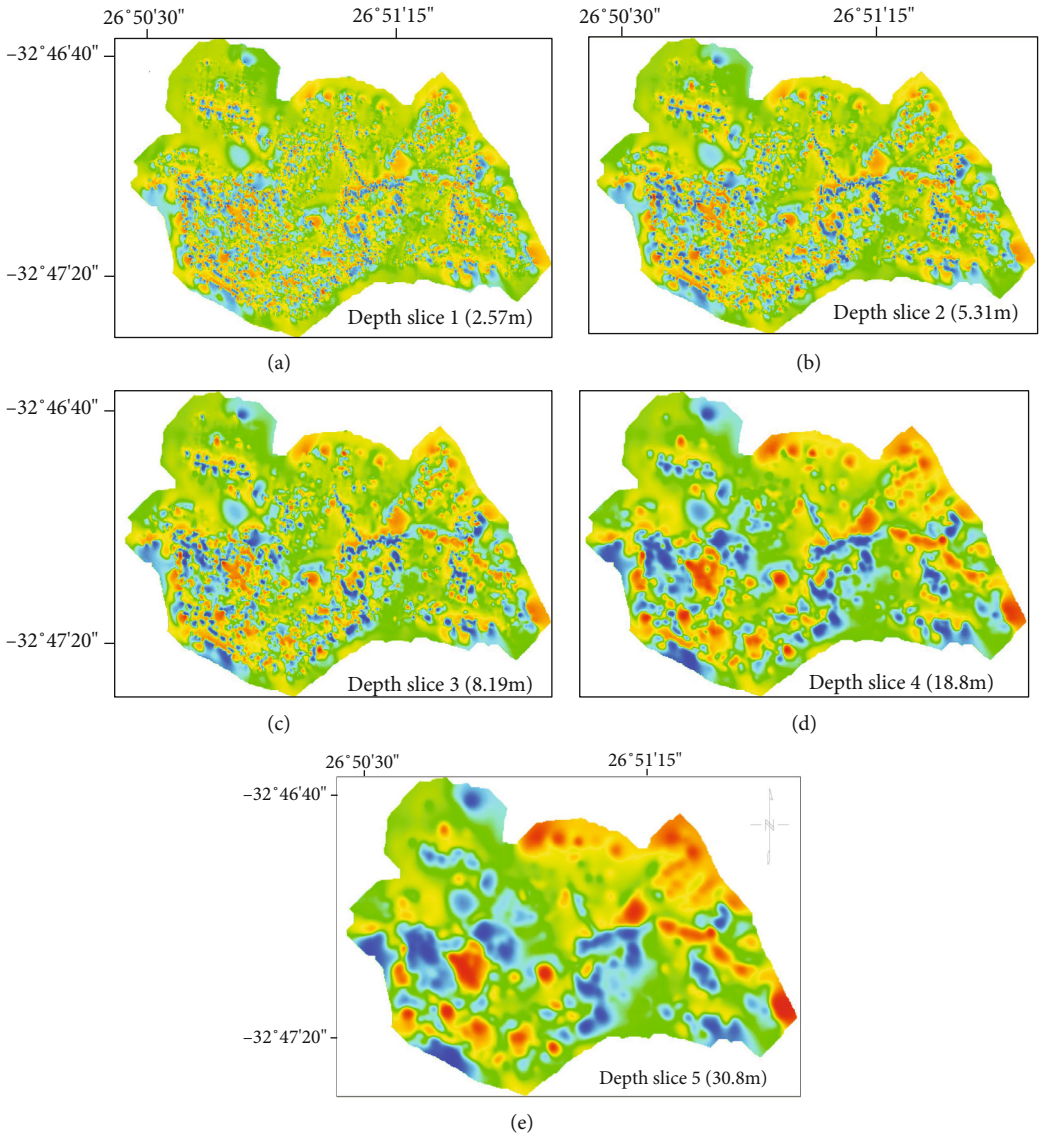


Figure 10: Magnetic depth slice maps: (a)–(e) are depth slices at depths of 2.57 m, 5.31 m, 8.19, 18.8 m, and 30.8 m, respectively.

*4.2.1. Geoelectric Models.* The apparent resistivity data obtained during the survey were inverted and interpreted qualitatively. The summary of the VES interpretation results is presented in Table 2. In this article, one representative VES curve from each category is presented (Figure 12). The HA curve type is denoted by VES modeled curve site 17 acquired along the University of Fort Hare Farm (Figure 12(a)). The curve begins with a top layer having a resistivity value of 31 Ωm and a thickness of 1.1 m. The resistivity of the second layer is 11 Ωm, and the thickness is 2.7 m, which is inferred to be mudstone. The third layer's resistivity is 136 Ωm, and its thickness is 30.2 m. This conductive layer is likely to be weathered/fractured sandstone. The fourth layer's resistivity is 5512 Ωm. The resistive fourth layer may be due to the presence of bedrock that has been unweathered. The thickness of the fourth layer is undefined, given that it is the last layer. The HK curve type is represented by VES modeled curve site 4 obtained along the University Cricket Field (Figure 12(b)). The surface terrain is composed of resistive topsoil (127 Ωm), and its thickness is 1.8 m. The second layer is 7.4 m thick and has a low resistivity value of 29 Ωm, which is inferred to be mudstone. The third layer is 72.6 m thick and has a resistivity value of 195 Ωm, which corresponds to sandstone. The resistivity value of the fourth layer is 112 Ωm, which corresponds to mudstone.

*4.2.2. Geoelectric Sections of the VES.* The VES results were used to prepare five geoelectric sections. The aim is to identify the aquifer horizon's geometry as well as the extent of the geoelectric layers in Alice. The geoelectric sections show the vertical and horizontal variations in lithology in accordance with the resistivity values in the subsurface resistivity values down to a depth of approximately 176.8 m. The geoelectric sections along the line in East Camp and Victoria Hospital Road are shown as examples in Figures 13(a) and 13(b).

The geoelectric section acquired along a line in East Camp is presented in Figure 13(a). The first layer, comprising the topsoil, occurs between depths of 1.0 and 1.4 m. The

Table 2: Summary of VES interpretation results.

| VES | Resistivity (Ωm) | | | | Thickness (m) | | | | Depth (m) | | | |
|---|---|---|---|---|---|---|---|---|---|---|---|---|
| | $\rho_1$ | $\rho_2$ | $\rho_3$ | $\rho_4$ | $h_1$ | $h_2$ | $h_3$ | $h_4$ | $d_1$ | $d_2$ | $d_3$ | $d_4$ |
| 1 | 169 | 7 | 237 | 44 | 1.1 | 4.9 | 47.4 | ∞ | 1.1 | 6.0 | 53.4 | ∞ |
| 2 | 152 | 11 | 182 | 53 | 1.0 | 5.0 | 51.7 | ∞ | 1.0 | 5.0 | 51.7 | ∞ |
| 3 | 228 | 28 | 155 | 117 | 1.3 | 7.4 | 61.4 | ∞ | 1.3 | 8.7 | 70.1 | ∞ |
| 4 | 127 | 29 | 195 | 112 | 1.8 | 7.4 | 72.6 | ∞ | 1.8 | 9.2 | 81.9 | ∞ |
| 5 | 166 | 42 | 179 | 177 | 1.4 | 17.5 | 143.9 | ∞ | 1.4 | 18.9 | 162.7 | ∞ |
| 6 | 15 | 4 | 291 | 860 | 1.3 | 3.6 | 23.3 | ∞ | 1.3 | 4.8 | 28.2 | ∞ |
| 7 | 11 | 5 | 720 | 241 | 1.6 | 2.6 | 128.1 | ∞ | 1.6 | 4.2 | 132.3 | ∞ |
| 8 | 35 | 6 | 295 | 714 | 1.2 | 4.4 | 41.8 | ∞ | 1.2 | 5.5 | 47.3 | ∞ |
| 9 | 161 | 8 | 958 | 263 | 1.0 | 5.3 | 113.2 | ∞ | 1.0 | 6.4 | 119.6 | ∞ |
| 10 | 271 | 17 | 6003 | 6640 | 1.1 | 9.1 | 52.8 | ∞ | 1.1 | 9.1 | 52.8 | ∞ |
| 11 | 126 | 21 | 931 | 677 | 1.0 | 7.1 | 13.5 | ∞ | 1.0 | 8.7 | 22.2 | ∞ |
| 12 | 233 | 27 | 188 | 456 | 1.1 | 7.6 | 66.3 | ∞ | 1.1 | 8.7 | 75.0 | ∞ |
| 13 | 214 | 33 | 296 | 501 | 1.0 | 8.7 | 71.0 | ∞ | 1.0 | 9.7 | 80.7 | ∞ |
| 14 | 199 | 32 | 289 | 452 | 1.0 | 10.8 | 98.0 | ∞ | 1.0 | 11.8 | 109.8 | ∞ |
| 15 | 174 | 24 | 206 | 299 | 1.3 | 5.9 | 66.4 | ∞ | 1.3 | 7.1 | 73.6 | ∞ |
| 16 | 20 | 8 | 941 | 2817 | 1.4 | 4.2 | 25.7 | ∞ | 1.4 | 5.6 | 31.3 | ∞ |
| 17 | 31 | 11 | 136 | 5512 | 1.1 | 2.7 | 30.2 | ∞ | 1.1 | 3.8 | 34.0 | ∞ |
| 18 | 30 | 14 | 137 | 5964 | 1.1 | 4.3 | 7.7 | ∞ | 1.1 | 5.4 | 13.1 | ∞ |
| 19 | 29 | 15 | 801 | 6589 | 1.2 | 5.9 | 17.4 | ∞ | 1.2 | 7.0 | 24.5 | ∞ |
| 20 | 24 | 13 | 7359 | 1716 | 1.2 | 4.0 | 171.6 | ∞ | 1.2 | 5.2 | 176.8 | ∞ |
| 21 | 107 | 8 | 781 | 2756 | 1.2 | 4.1 | 22.5 | ∞ | 1.2 | 5.3 | 27.8 | ∞ |
| 22 | 74 | 40 | 387 | 1324 | 1.0 | 1.4 | 59.7 | ∞ | 1.0 | 2.4 | 62.1 | ∞ |
| 23 | 68 | 27 | 1333 | 1361 | 1.3 | 2.1 | 44.7 | ∞ | 1.3 | 3.4 | 51.1 | ∞ |
| 24 | 74 | 31 | 3415 | 2008 | 1.2 | 2.7 | 118.6 | ∞ | 1.2 | 3.9 | 122.5 | ∞ |
| 25 | 24 | 49 | 2825 | 60428 | 1.4 | 0.9 | 4.8 | ∞ | 1.4 | 2.3 | 7.1 | ∞ |

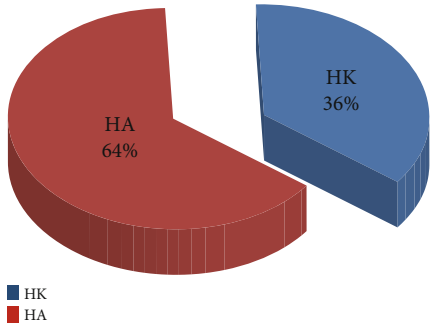


Figure 11: Pie chart showing the VES curve types present in the study area.

second layer indicates clay from 2.3 m to 5 m, and the third layer, a weathered/fractured sandstone, occurs between 7 m and 123 m. The last layer possibly consists of dolerite, and its depth is undefined, given that it is the last layer. Likewise, the geoelectric section acquired along Victoria Hospital Road in Figure 13(b) shows that the first layer is 1.0 m to 1.3 m thick and consists of topsoil. The second layer, made up of mudstone, varies in depth between 9 m and 12 m. The third layer is made up of weathered/fractured sandstone with a depth ranging between 22 m and 110 m. The fourth layer consists of sandstones that have been weathered and occur further than 100 m. VES station 14 is situated between two fault planes.

## 5. Discussion

*5.1. Magnetic.* The maximum and minimum anomaly frequencies, which are connected to the local distribution of magnetization, are displayed by the magnetic maps. A change in magnetic susceptibility generally implies that the rock's composition has changed [60]. Magnetic anomalies are shown on magnetic maps based on their characteristics and structure. [61] states that the shapes of the anomalies enable the identification of the fundamental geological features of the buried source. The RTP magnetic map of the study area shows different regions of low and high intensity. The low magnetic regions consist of rocks with low magnetic susceptibility, situated in Alice's central and southwest parts. The high magnetic zones, mainly the northeastern and southwestern parts, occur owing to magnetic sources at depth [59] and are inferred to be Karoo dolerite intrusions. According to [62], the RTP map's high-gradient regions may suggest the occurrence of high-gradient zones. [63]

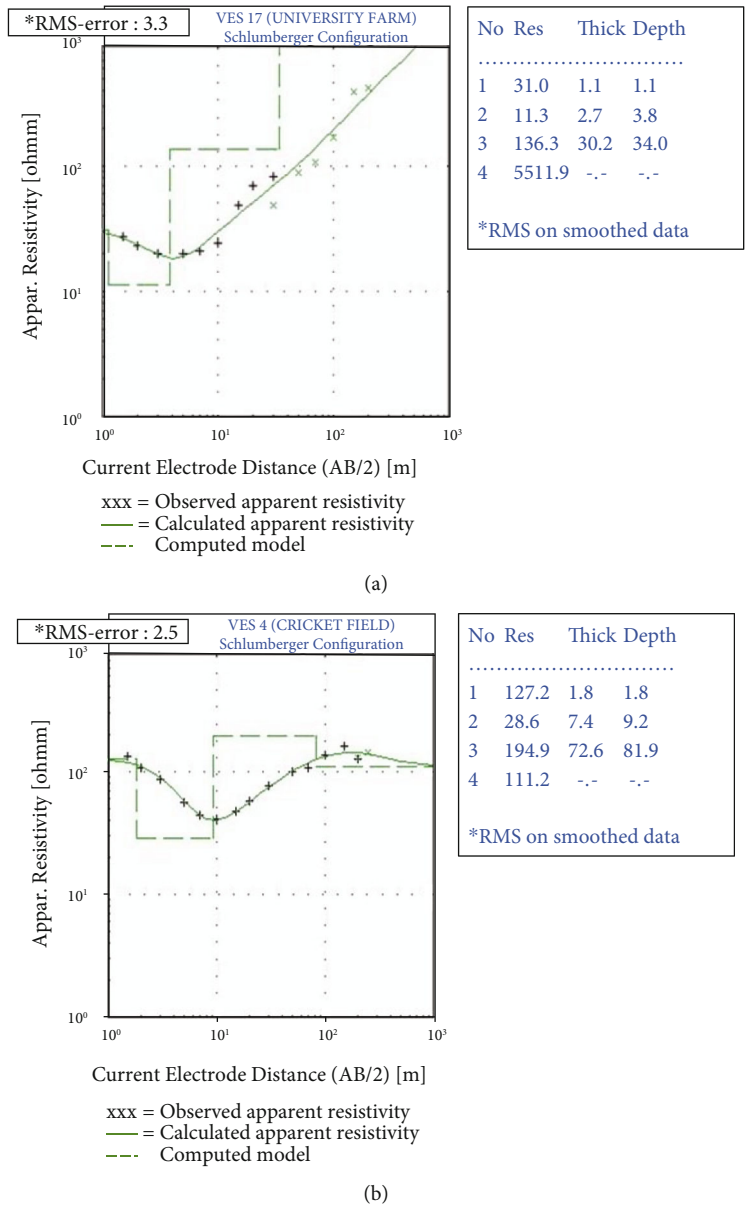


Figure 12: VES representative curves of the HA curve type (a) and HK curve type (b).

documents that knowing the geometry and distribution of the Karoo dolerite will assist groundwater exploration companies in drilling wells to intersect the dolerite-dominated areas. Hence, the THD map reveals several dolerite intrusions (dykes and sills), which may be targeted for potential groundwater exploration. Several researchers [26, 64, 65] have documented that most boreholes drilled alongside linear geological structures, mainly dolerite dykes, are more productive than those drilled away from geological structures.

Meanwhile, there is a positive correlation between the low magnetic areas seen on the RTP map and the location of the dolerite intrusions on the THD map, which implies that the low magnetic intensity of RTP possibly represents the area of occurrence of dolerite dykes and sills on the THD map. This finding aligns with [66], who stated that the dolerites are embedded in neotectonic fractures. However, the significant aquifer in the Karoo is anticipated to have low yield and permeability at the contact area of host rocks and dolerites, which aligns with the reports of [16, 65]. The aquifer system in Alice is possibly hosted in the sedimentary rocks within the Daggaboersnek Member of the Karoo Supergroup [26, 37].

[28] conducted research that focuses on characterizing, borehole drilling, and measuring the flow parameters of the rock aquifer system within the current study area. Superimposed on the AS map are the two (2) drilled borehole points in the study area (Figure 14). The boreholes are sited in the NE region. This was done to evaluate the correlation between geological features (sills and dykes) and the borehole locations to examine the influence of these geological features on groundwater flow using the borehole data.

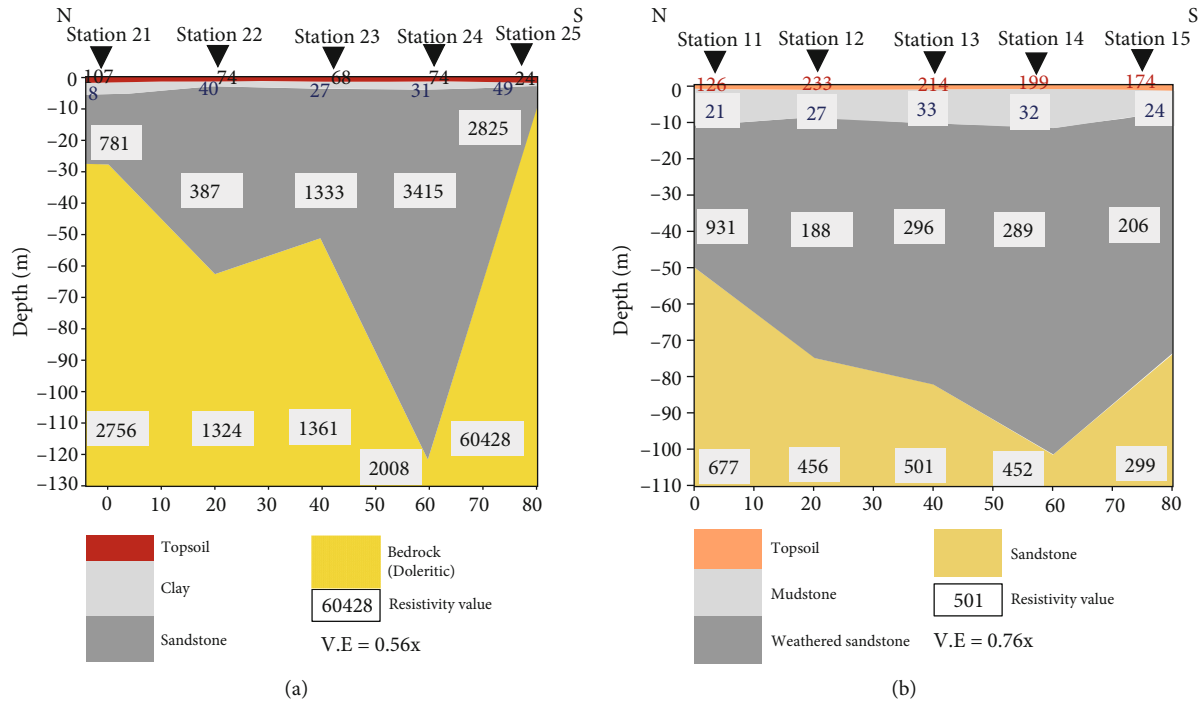


Figure 13: Geoelectric sections acquired along a line in (a) East Camp and (b) Victoria Hospital Road (V.E. means vertical exaggeration).

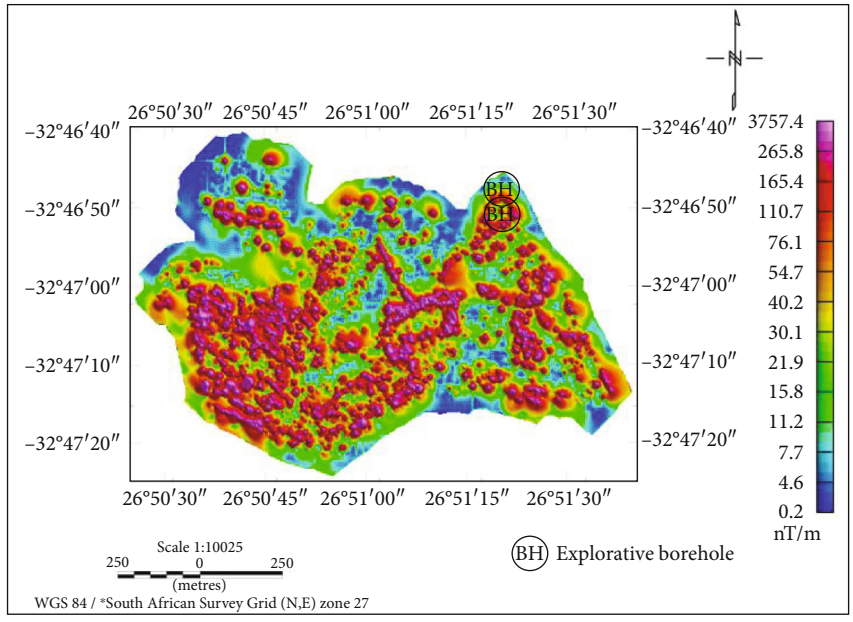


Figure 14: Overlay of the two boreholes on the analytical signal map of Alice for correlation purposes.

During the drilling, four water strikes occurred at depths of 8, 22, 54, and 65 m. The blow yield from both boreholes was 24000 l/h at a depth of 54 m. Due to the maximum flow yields at this level, the boreholes might be interconnected through fractures. Both boreholes gave a higher flow yield of 36000 l/h at a depth of 65 m, implying that there may be another fracture connecting the two boreholes. It appears that the formation may be extensively fractured because it is extremely loose between depths of 54 and 65 m.

Figure 14 shows that the boreholes are drilled on a sill-like structure in the NE part. Meanwhile, [64] noted that fracturing might be improved at the bottom of curving sills or dyke–sill intersection points, thus influencing the migration and distribution of groundwater. Therefore, the loose formation and the high blow yield noted at depths of 54 and 65 m indicated that the boreholes might have been drilled through a fracture caused by the dolerite intrusion. The finding aligns with [14], who posited that the dolerite intrusion in the study area caused the area's formation to

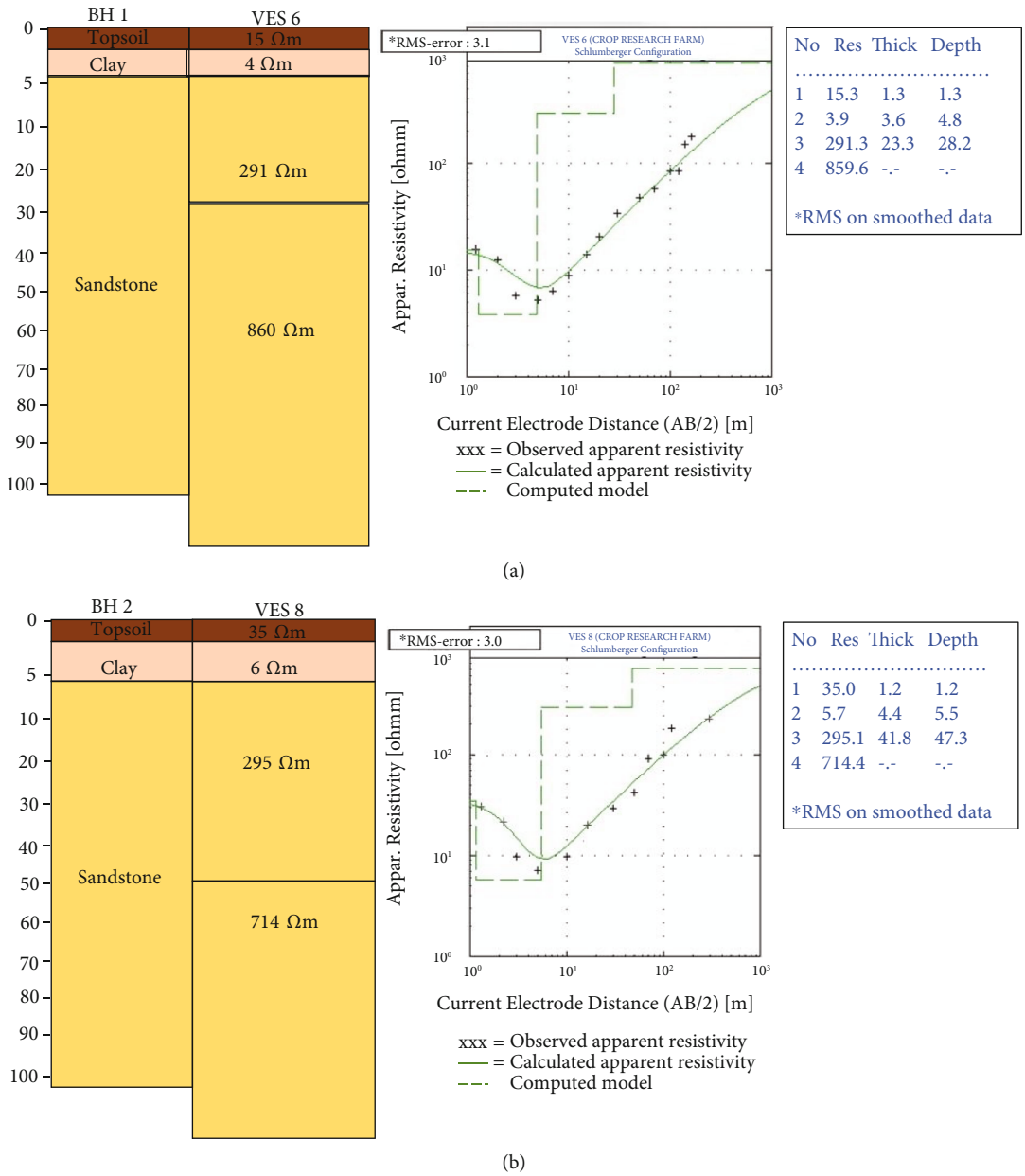


Figure 15: (a) Correlation between BH 1 and VES 6. (b) Correlation between BH 2 and VES 8.

be extensively fractured, which made them suitable aquifers due to secondary permeability. In addition, it was noted that the Permian mudstones and sandstones serve as the primary aquifers in the Karoo Basin, as well as the dolerite dykes and sills. Furthermore, the finding on the high blow yield due to boreholes drilled through the fracture aligns with the report of [67] on the positive yield analysis of boreholes drilled into a fractured structure.

*5.2. Electrical Resistivity.* The interpretation of the geoelectrical data of VES shows two types of sounding curves, indicating the arrangement of geological layers and their electrical characteristics. The geological layer models are composed of topsoil (0.4–1.8 m; 20-5752 Ωm), a second layer (0.8–17.5 m; 3-51 Ωm), the third layer (2.1–171.6 m; 136-7359 Ωm), and bedrock layer (44 to 60428 Ωm). According to the classification of several well-known rocks using resistivity values given by [68], layers having low resistivity (1–20 Ωm) in the study area could probably be associated with clay, and the intermediate resistivity layers (20–5000 Ωm) could be related to mudstone and sandstone. High resistivity values (>5000 Ωm) of the bedrock observed are associated with sediments found in the Balfour Formation, which were intruded by dolerites [27].

In addition, the findings on outcrops and data from past studies [26, 28, 34, 36, 37, 40] aided in designing the lithological 1D models associated with each sounding curve using the 1D geoelectrical models generated. Therefore, it is acknowledged that the study area shows various lithological models composed of different types of sedimentary rocks

(sandstone, mudstone, and clays, which are intruded by dolerites) [40]. The findings align with [34], who stated that the Balfour Formation comprises sedimentary rocks, like sandstone, shale, mudstone, and alternating siltstone.

The lithological 1D models from the HA- and HK-type curves from the study area show that a viable aquifer could be found in the third layer, which has resistivity values between 136 and 352 Ωm, 9.9 to 172 m thick, and depths ranging from 16.1 to 163 m. This third layer comprises sandstone and mudstone, in which the major substantial aquifers located within the Karoo Supergroup are found [26, 28, 34, 37]. In the geoelectric section (Figure 13(a)), the sandstone layer is more pronounced and, in some places, intruded by dolerites. The noticeable deformation brought on by the dolerites present in the Karoo enhances the permeability of its aquifer system in the contact areas of the dyke. In VES 24 and 25, the dolerite intruded almost to the surface of this layer. The two VES stations are situated near Somgxada Mountain in the study area.

The geoelectric section shows an electrical discontinuity between VES stations 21 and 23, which could be caused by the passage of a fault that influences the aquifer's groundwater flow. The low gaps between high resistive bodies indicate fault regions that may serve as paths for groundwater passage, thus increasing groundwater localization [68]. Similarly, [69] posited that fault zones have excellent storage capacity and are highly productive. The aquifer around VES 22 lies within the weathered/fractured sandstone, about 59.7 m thick, with a depth of 62 m. The deepest aquifer at approximately 110 m depth could be seen at VES station 14 (Figure 13(b)). This VES 14 station aquifer seems preferable for groundwater exploitation because of its greater depth and low resistivity value. The geoelectric sections (Figures 13(a) and 13(b)) show that the aquifer zone could be found in the third layer (i.e., sandstone). The finding corroborates the results of [16], who suggested that the most important type of aquifers found in the Karoo are developed in weathered sedimentary rocks (sandstone, mudstone, siltstone, and shale) characterized by low permeability.

To enable the lithocorrelation, two vertical electrical soundings (VES 6 and VES 8) were located beside two boreholes (BH1 and BH2). The geoelectric models and sections were created using other VES stations. The resistivity records of VES 6 and 8 show a high correspondence with the borehole data of BH1 and BH 2 (Figures 15(a) and 15(b)), where the lithology at a depth of 28 m at the borehole BH1 is sandstone and at VES 6 is sandstone. The depth of the sandstone aquifer at VES 8 is above 48 m, while borehole BH2 strikes the water at depths of 54 and 66 m. Therefore, the results of the geoelectrical data correlated well with the borehole log data from the study area's boreholes drilled by [28].

## 6. Conclusions

This research shows the vital contribution of the magnetic and resistivity methods as a practical tool for investigating potential groundwater zones in Alice, Eastern Cape, South Africa, and other areas where applicable. The ground magnetic results show that the anomaly signature amplitudes vary, suggesting that the magnetic body source is not uniformly distributed along each profile across the study area. The variation between positive and negative magnetic anomalies indicates the presence of subsurface lineaments, which may influence the groundwater movement in the study area. As observed on the magnetic depth slice maps, the magnetic anomalies become broader up to the depth of 18.8 m and later fade away at a depth of around 31 m. This finding suggests that Karoo dolerite intrusions were intruded close to the surface. According to the findings of the VES, the subsurface is composed of four layers of HK and HA types that characterize the types of sounding curves and the vertical changes in Alice. From the results of the VES curves, 15 VES stations (VES 1, 2, 3, 4, 5, 6, 7, 8, 9, 12, 13, 14, 15, 17, and 22) are selected as potential groundwater zones, with aquifer layer resistivity values between 136 and 352 Ωm. The thickness of the aquifer layer varies between 9.9 and 143.9 m, with depths between 16.1 and 163 m. The aquifer zone is inferred to be the third layer, and the depth of the aquifer zone is considered between 30 and 160 m. However, it is recommended that water should be collected from each successful borehole for bacteriological and physicochemical tests to ensure that the water is safe and suitable for various purposes. The results from the geoelectric sections further revealed areas of weakness, interpreted as weathered/fractured zones accountable for groundwater accumulation in the study area. Low resistivity zones indicate highly faulted and weathered/fractured zones; therefore, they are suitable for groundwater storage. Meanwhile, high resistivities are linked to dolerite intrusions. The borehole lithologic log correlated well with the magnetic and electrical resistivity survey results. Thus, these geophysical methods are efficient in locating potential groundwater zones. The results will guide the drilling of boreholes aiming to harness the groundwater resources in Alice.

## Data Availability

The data used in this research are available upon request at the Department of Geology, University of Fort Hare, South Africa, and from the corresponding author.

## Conflicts of Interest

The authors declare that they have no conflicts of interest.

## Acknowledgments

We thank Professor Christopher Baiyegunhi (University of Limpopo) for his valuable comments and constructive criticism. The research was funded by the DSI-NRF CIMERA (Centre of Excellence for Integrated Mineral and Energy Resource) of South Africa and Govan Mbeki Research and Development Centre (GMRDC) of the University of Fort Hare. Open access funding is enabled and organized by SANLiC Gold.

## References


[1] N. Hernández-Mora, L. Martınez-Cortina, and J. Fornés, *Intensive Groundwater Aquifer Over-exploitation. Implications for Water Policy in Southern Europe. Agricultural Use of Groundwater. Towards Integration between Agricultural Policy and Water Resources Management, Kluwer*, Academic Publishers, 2001.

[2] F. Yang, P. Gao, D. Li, H. Ma, and G. Cheng, "Application of comprehensive geophysical prospecting method in groundwater exploration," *IOP Conference Series: Earth and Environmental Science*, vol. 108, article 032022, 2018.

[3] A. O. Lawrence and T. A. Ojo, "The use of combined geophysical survey methods for groundwater prospecting in a typical basement complex terrain: case study of Ado-Ekiti Southwest Nigeria," *Research Journal in Engineering and Applied Sciences*, vol. 1, no. 6, pp. 362–376, 2012.

[4] S. A. Ngah and H. O. Nwankwoala, "Geophysical logging of a borehole for supply of potable groundwater at Opuama community, Warri North LGA, Delta State, Nigeria," *New York Science Journal*, vol. 9, no. 10, pp. 83–88, 2016.

[5] K. A. Salako, A. A. Adetona, U. D. Alhassan, A. A. Rafiu, N. P. Ofor, and E. E. Udensi, *Vertical Electrical Sounding Investigation for Groundwater at the South-Western Part of (Site A) of Nigerian Mobile Police Barracks (Mopol 12), David Mark Road, Maitumbi, Minna*, J of Science Education and Technology, 2009.

[6] World Economic Forum, *World Economic Forum Annual Meeting*, 2014, https://www.weforum.org/events/world-economic-forum-annual-meeting-2014.

[7] R. R. A. M. Mato, *Groundwater Pollution in Urban Dar es Salaam, Tanzania: Assessing vulnerability and protection priorities*, University College of Lands and Architectural Studies, Dar es Salaam, Tanzania, 2004.

[8] T. H. Y. Tebbutt, *Principles of water quality control*, Elsevier, 1998.

[9] H. Pienaar, Y. Xu, E. Braune, J. Cao, S. Dzikiti, and N. Z. Jovanovic, "Implementation of groundwater protection measures, particularly resource-directed measures in South Africa: a review paper," *Water Policy*, vol. 23, no. 4, pp. 819–837, 2021.

[10] J. D. S. Cullis, A. H. M. Gorgens, and C. Marais, "A strategic study of the impact of invasive alien plants in the high rainfall catchments and riparian zones of South Africa on total surface water yield," *Water SA*, vol. 33, no. 1, pp. 35–42, 2009.

[11] L. Van Vuuren, "Water resource management: drought management-strengthening our knowledge armoury," *Water Wheel*, vol. 14, no. 6, pp. 14–17, 2015.

[12] T. M. Urban, D. D. Anderson, and W. W. Anderson, "Multimethod geophysical investigations at an Inupiaq village site in Kobuk Valley, Alaska," *The Leading Edge*, vol. 31, no. 8, pp. 950–956, 2012.

[13] W. J. Seaton and T. J. Burbey, "Evaluation of two-dimensional resistivity methods in a fractured crystalline- rock terrane," *Journal of Applied Geophysics*, vol. 51, no. 1, pp. 21–41, 2002.

[14] S. Adams, R. Titus, K. Pietersen, G. Tredoux, and C. Harris, "Hydrochemical characteristics of aquifers near Sutherland in the Western Karoo, South Africa," *Journal of Hydrology*, vol. 241, no. 1-2, pp. 91–103, 2001.

[15] F. D. Day-Lewis, J. W. Lane, and S. M. Gorelick, "Combined interpretation of radar, hydraulic, and tracer data from a fractured-rock aquifer near Mirror Lake, New Hampshire, USA," *Hydrogeology Journal*, vol. 14, no. 1-2, pp. 1–14, 2006.

[16] B. H. Usher, J. A. Pretorius, and G. J. Van Tonder, "Management of a Karoo fractured-rock aquifer system-Kalkveld water user association (WUA)," *Water SA*, vol. 32, no. 1, pp. 9–19, 2007.

[17] A. Khashaba, M. Mekkawi, E. Ghamry, and E. Abdel Aal, "Land magnetic investigation on the west Qarun oil field, western Desert-Egypt," *Journal of Geological Geophysics*, vol. 6, no. 1, 2017.

[18] G. K. Anudu, R. A. Stephenson, and D. I. Macdonald, "Using high-resolution aeromagnetic data to recognise and map intra-sedimentary volcanic rocks and geological structures across the Cretaceous middle Benue Trough, Nigeria," *Journal of African Earth Sciences*, vol. 99, pp. 625–636, 2014.

[19] I. M. Ibraheem, E. A. Elawadi, and G. M. El-Qady, "Structural interpretation of aeromagnetic data for the Wadi El Natrun area, northwestern desert, Egypt," *Journal of African Earth Sciences*, vol. 139, pp. 14–25, 2018.

[20] F. H. AL-Menshed and J. M. Thabit, "Comparison between VES and 2D imaging techniques for delineating subsurface plume of hydrocarbon contaminated water southeast of Karbala City, Iraq," *Arabian Journal of Geosciences*, vol. 11, no. 7, pp. 1–9, 2018.

[21] S. M. Sharafeldin, K. S. Essa, M. A. Youssef, H. Karsli, Z. E. Diab, and N. Sayil, "Shallow geophysical techniques to investigate the groundwater table at the Great Pyramids of Giza, Egypt," *Geoscientific Instrumentation, Methods and Data Systems*, vol. 8, no. 1, pp. 29–43, 2019.

[22] R. Stanly, S. Yasala, and R. V. Murugesan, "Hydrological subsurface investigation using geophysical electrical and magnetic methods in and around Valliyar river basin, India," *Results in Geophysical Sciences*, vol. 7, article 100022, 2021.

[23] A. I. Riwayat, M. A. A. Nazri, and M. H. Z. Abidin, "Application of electrical resistivity method (ERM) in groundwater exploration," *Journal of Physics: Conference Series*, vol. 995, article 012094, 2018.

[24] E. S. Joel, P. I. Olasehinde, T. A. Adagunodo, M. Omeje, M. L. Akinyemi, and J. S. Ojo, "Integration of aeromagnetic and electrical resistivity imaging for groundwater potential assessments of coastal plain sands area of Ado-Odo/Ota in Southwest Nigeria," *Groundwater for Sustainable Development*, vol. 9, article 100264, 2019.

[25] M. O. Olorunfemi and A. G. Oni, "Integrated geophysical methods and techniques for siting productive boreholes in basement complex terrain of southwestern Nigeria," *Ife Journal of Science*, vol. 21, no. 1, pp. 13–26, 2019.

[26] A. C. Woodford and L. P. Chevallier, *Regional characterization and mapping of Karoo fractured aquifer systems: an integrated approach using a geographical information system and digital image processing*, Water Research Commission, 2002.

[27] S. Mepaiyeda, K. Madi, O. Gwavava, C. Baiyegunhi, and L. Sigabi, "Contaminant delineation of a landfill site using electrical resistivity and induced polarization methods in Alice, Eastern Cape, South Africa," *International Journal of Geophysics*, vol. 2019, Article ID 5057832, 13 pages, 2019.

[28] L. Yu, *Measurement of the Bulk Flow and Transport Characteristics of Selected Fractured Rock Aquifer Systems in South Africa: A Case Study of the Balfour Formation in the Eastern Cape Province, [M.S. thesis]*, University of Fort Hare, Alice, South Africa, 2011.

[29] O. Catuneanu, H. Wopfner, P. G. Eriksson et al., "The Karoo basins of south-central Africa," *Journal of African Earth Sciences*, vol. 43, no. 1-3, pp. 211–253, 2005.

[30] C. Baiyegunhi and O. Gwavava, "Magnetic investigation and 2½ D gravity profile modelling across the Beattie magnetic anomaly in the southeastern Karoo Basin, South Africa," *Acta Geophysica*, vol. 65, no. 1, pp. 119–138, 2017.

[31] O. Catuneanu, P. J. Hancox, and B. S. Rubidge, "Reciprocal flexural behaviour and contrasting stratigraphies: a new basin development model for the Karoo retroarc foreland system, South Africa," *Basin Research*, vol. 10, no. 4, pp. 417–439, 1998.

[32] R. M. H. Smith, P. G. Eriksson, and W. J. Botha, "A review of the stratigraphy and sedimentary environments of the Karoo-aged basins of Southern Africa," *Journal of African Earth Sciences*, vol. 16, no. 1-2, pp. 143–169, 1993.

[33] C. Baiyegunhi and K. Liu, "Sedimentary facies, stratigraphy, and depositional environments of the Ecca group, Karoo Supergroup in the Eastern Cape Province of South Africa," *Open Geosciences*, vol. 13, no. 1, pp. 748–781, 2021.

[34] M. E. Oghenekome, *Sedimentary Environments and Provenance of the Balfour Formation (Beaufort Group) in the Area between Bedford and Adelaide, Eastern Cape Province, South Africa, [M.S. thesis]*, University of Fort Hare, Alice, South Africa, 2012.

[35] C. A. Haycock, T. R. Mason, and M. K. Watkeys, "Early Triassic palaeoenvironments in the eastern Karoo foreland basin, South Africa," *Journal of African Earth Sciences*, vol. 24, no. 1-2, pp. 79–94, 1997.

[36] O. Catuneanu and H. N. Elango, "Tectonic control on fluvial styles: the Balfour formation of the Karoo Basin, South Africa," *Sedimentary Geology*, vol. 140, no. 3-4, pp. 291–313, 2001.

[37] D. Katemaunzanga and G. J. Gunter, "Lithostratigraphy, sedimentology and provenance of the Balfour formation, Beaufort Group in the Fort Beaufort Alice area, Eastern Cape Province, South Africa," *Acta Geologica Sinica - English Edition*, vol. 83, no. 5, pp. 902–916, 2009.

[38] B. H. Usher, J. A. Pretorius, and G. J. Van Tonder, *Establishment of a Groundwater Management Plan for Kalkveld*, Unpublished report prepared for DWAF, Free State Region, 2004.

[39] C. Baiyegunhi and O. Gwavava, "Variations in isochore thickness of the Ecca sediments in the eastern Cape Province of South Africa, as deduced from gravity models," *Acta Geologica Sinica - English Edition*, vol. 90, no. 5, pp. 1699–1712, 2016.

[40] M. R. Johnson, C. J. Van Vuuren, J. N. Visser et al., *Sedimentary rocks of the Karoo Supergroup*, Geological Society of South Africa, Johannesburg/Council for Geosciences, Pretoria, 2006.

[41] C. Baiyegunhi, K. Liu, and O. Gwavava, "Diagenesis and reservoir properties of the Permian Ecca Group sandstones and mudrocks in the Eastern Cape Province, South Africa," *Minerals*, vol. 7, no. 6, p. 88, 2017.

[42] A. G. Oni, P. J. Eniola, M. O. Olorunfemi, M. O. Okunubi, and G. A. Osotuyi, "The magnetic method as a tool in groundwater investigation in a basement complex terrain: Modomo Southwest Nigeria as a case study," *Applied Water Science*, vol. 10, no. 8, pp. 1–18, 2020.

[43] N. W. Peddie, "International geomagnetic reference field the third generation," *Journal of Geomagnetism and Geoelectricity*, vol. 34, no. 6, pp. 309–326, 1982.

[44] L. Guo, L. Shi, and X. Meng, "The antisymmetric factor method for magnetic reduction to the pole at low latitudes," *Journal of Applied Geophysics*, vol. 92, pp. 103–109, 2013.

[45] B. McKenzie, C. Foss, and D. Hillan, "Issues related to determination of the horizontal centre of magnetization," *ASEG Extended Abstracts*, vol. 2012, no. 1, pp. 1–4, 2012.

[46] W. N. MacLeod, D. C. Turner, and E. P. Wright, *The geology of the Jos plateau, geological survey of Nigeria*, Ministry of Mines and Power, 1972.

[47] M. Pilkington and P. Keating, "Contact mapping from gridded magnetic data? A comparison of techniques," *Exploration Geophysics*, vol. 35, no. 4, pp. 306–311, 2004.

[48] Y. Jeng, Y. L. Lee, C. Y. Chen, and M. J. Lin, "Integrated signal enhancements in magnetic investigation in archaeology," *Journal of Applied Geophysics*, vol. 53, no. 1, pp. 31–48, 2003.

[49] G. R. J. Cooper and D. R. Cowan, "Filtering using variable order vertical derivatives," *Computers & Geosciences*, vol. 30, no. 5, pp. 455–459, 2004.

[50] S. T. Owolabi, K. Madi, A. M. Kalumba, and C. Baiyegunhi, "A geomagnetic analysis for lineament detection and lithologic characterization impacting groundwater prospecting; a case study of Buffalo catchment, Eastern Cape, South Africa," *Groundwater for Sustainable Development*, vol. 12, article 100531, 2021.

[51] A. Christensen and M. Dransfield, "Airborne vector magnetometry over banded iron formations," in *72nd Annual international meeting of Society of Exploration Geophysics*, pp. 13–16, Salt Lake City, Utah, 2002.

[52] J. D. Phillips, "Locating magnetic contacts: a comparison of the horizontal gradient, analytical signal and local wavenumber methods," in *70th Annual international meeting, SEG, expanded abstracts*, pp. 402–405, Calgary, Canada, 2000.

[53] E. Hassan, J. K. Rai, and U. O. Anekwe, "Geoelectrical survey of ground water in some parts of Kebbi state Nigeria, a case study of Federal Polytechnic Bye-Pass Birnin Kebbi and Magoro Primary Health Center Fakai Local Government," *Geosciences*, vol. 7, no. 5, pp. 141–149, 2017.

[54] J. M. Reynolds, *An Introduction to Applied and Environmental Geophysics*, John Wiley and Sons, NY, USA, 1997.

[55] D. S. Parasnis, *Principles of Applied Geophysics*, Chapman and Hall, London, England, 1997.

[56] H. P. Patrax and S. K. Nath, *Schlumberger geoelectric sounding in groundwater, Principles, Interpretation and Application*, A. A. Balkema Publishers, USA, 1998.

[57] O. Koefoed, *Geosounding Principles, 1. Resistivity sounding measurements*, Elsevier Scientific Publishing, 1979.

[58] M. H. Loke, *Tutorial: 2-D and 3-D electrical imaging surveys*, 2004, http://www.geomom.com.

[59] C. Baiyegunhi, O. Gwavava, K. Liu, and T. L. Oloniniyi, "An integrated geophysical approach to mapping and modeling the Karoo dolerite intrusions in the southeastern Karoo Basin of South Africa," in *SEG Technical Program Expanded Abstracts*, pp. 1474–1478, Society of Exploration Geophysicists, 2018.

[60] H. Ugalde and B. Morris, "Cluster analysis of Euler deconvolution solutions: new filtering techniques and actual link to geological structure," in *2008 SEG annual meeting*, One Petro, 2008.

[61] K. S. Essa and M. Elhussein, "Magnetic interpretation utilizing a new inverse algorithm for assessing the parameters of buried inclined dike-like geological structure," *Acta Geophysica*, vol. 67, no. 2, pp. 533–544, 2019.

[62] S. A. Araffa, M. I. Mohamadin, H. Saleh Sabet, and M. S. Takey, "Geophysical interpretation for groundwater exploration around Hurghada area, Egypt," *NRIAG Journal of Astronomy and Geophysics*, vol. 8, no. 1, pp. 171–179, 2019.

[63] L. P. Chevallier, M. L. Goedhart, and A. C. Woodford, *Influence of Dolerite Sill and Ring Complexes on the Occurrence of*

*Groundwater in Karoo Fractured Aquifers: A Morpho-Tectonic Approach: Report to the Water Research Commission*, Water Research Commission, 2001.

[64] K. Senger, S. J. Buckley, L. Chevallier et al., "Fracturing of doleritic intrusions and associated contact zones: implications for fluid flow in volcanic basins," *Journal of African Earth Sciences*, vol. 102, pp. 70–85, 2015.

[65] S. T. Owolabi, K. Madi, A. M. Kalumba, and I. R. Orimoloye, "A groundwater potential zone mapping approach for semi-arid environments using remote sensing (RS), geographic information system (GIS), and analytical hierarchical process (AHP) techniques: a case study of Buffalo catchment, Eastern Cape, South Africa," *Arabian Journal of Geosciences*, vol. 13, no. 22, pp. 1–17, 2020.

[66] L. Chevallier and A. Woodford, "Morpho-tectonics and mechanism of emplacement of the dolerite rings and sills of the western Karoo, South Africa," *South African Journal of Geology*, vol. 102, no. 1, pp. 43–54, 1999.

[67] R. Meyer, G. Le Roux, and M. Dindar, *Guidelines for the Monitoring and Management of Ground Water Resources in Rural Water Supply Schemes*, Water Research Commission, 2002.

[68] M. Mpofu, K. Madi, and O. Gwavava, "Remote sensing, geological, and geophysical investigation in the area of Ndlambe municipality, Eastern Cape Province, South Africa: implications for groundwater potential," *issue*, vol. 11, article 100431, 2020.

[69] K. Pietersen, H. E. Beekman, and M. Holland, *South African groundwater governance case study. In: Report Prepared for the World Bank in Partnership with the South African Department Groundwater Issues in Hard Rock & Geophysics of Water Affairs and the Water Research Commission*, WRC Report No. KV 273/11, 2011.